



An Investigation on the Impact of the Interpass-Cooling Time on the Metallurgy of Wire-Arc-Additive-Manufacturing SS308L Components

Van Thao Le^(✉) and Van Tao Le

Advanced Technology Center, Le Quy Don Technical University,
Hanoi, Vietnam

Abstract. In this paper, we focused on observing the influence of the interpass-cooling time on the microstructure of stainless steel (SS308L) walls fabricated by the wire and arc additive manufacturing (WAAM) process. For this purpose, two SS308L walls were produced by WAAM according to the unidirectional depositing strategy with an interpass-cooling time of 30 (s) and 60 (s) between two consecutively deposited layers. The findings indicate that in terms of microstructures there is no significant difference between two as-built thin walls. The microstructure of WAAM SS308L walls contains dominant austenite phases and a small amount of ferrite, which exists in the boundaries of austenite grains. However, when the interlayer idle time increases the secondary dendrite arm spacing (SDAS) becomes narrow, resulting in an augmentation in the microhardness and tensile properties of as-built components.

Keywords: Wire-arc-additive-manufacturing (WAAM) · Interpass-cooling time · 308L steel · Metallurgy

1 Introduction

WAAM - wire arc additive manufacturing is known as a metal-based additive manufacturing (AM) technology, in which the arc is used as the energy source to melt metal wire and fabricates metal parts layer-by-layer. In comparison to other metal AM technologies, this technique features high rate of production and low costs of device investment [1]. Therefore, WAAM is considered as an excellent-technological option to build large-scale components. However, the main drawback of such a technique is that the heat accumulation in WAAM parts is very high. This is due to the high heat input generated by the arc source and reheating cycles during the WAAM process [2]. Therefore, high thermal distortion and stress is one of the most crucial issues related to WAAM as-built components. To reduce the heat accumulation, the interpass-cooling time between successive deposits is generally used [3–5]. The interpass-cooling time enables cooling down the workpiece before the deposit of the next layer.

In the current paper, the impact of the interpass-cooling time on metallurgical characteristics of stainless steel (SS308L) walls built by WAAM was explored. From

the findings obtained in this study, we can select an effective interpass-cooling time for the production of WAAM SS308L components.

2 Experiments

In the current work, two stainless steel (SS308L) walls had been manufactured from the commercial SS308L wire by using a robotic welding system (Fig. 1a) according to the unidirectional depositing direction strategy (Fig. 1b). The wire has a diameter of 1 mm, and its chemical composition contains (19.5–21)% Cr and (9.0–11.0)% Ni. The percentage of C, P, and S is inferior to 0.03%. The processing parameters employed to produce the walls were presented in Table 1 [6].

Table 1. Processing conditions employed in experiments.

Process parameter	Value and unit
Welding current, I	122 (A)
Voltage, U	20 (V)
Traveling speed, v	0.368 (m/min)
Flow rate of the shielding gas	15 (L/min)
Interpass-cooling time	30 (s) for the first wall, 60 (s) for the second wall

The length of each deposit is 120 mm and each wall consists of 18 deposited layers. During the depositing process, a gas (99.9% of argon) was employed to protect the molten pool against the ambiance. The flow rate of the shielding gas is 15 l/min. In addition, an interpass-cooling time (T_{id}) of 30 s and 60 s between two successive deposits was applied during the build of the first and the second wall, respectively, for the free cooling purpose.

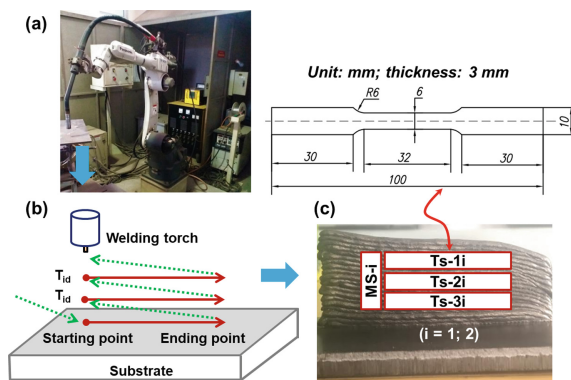


Fig. 1. The welding robot (a), the unidirectional depositing strategy (b), and (c) the built wall with the locations to extract metallurgical and tensile samples.

To compare the impact of different interpass-cooling times on the metallurgical properties, the material of as-built walls in the middle region was taken into consideration. In each case, a metallurgical sample (MS-*i*) and 03 tensile samples (Ts-1*i*, Ts-2*i*, and Ts-3*i*) in the horizontal direction had been prepared (Fig. 1c), where $i = \{1; 2\}$ for the first wall and the second wall, respectively.

To observe the microstructure of the walls, an AXIO imager A2M was used. The micro-hardness was tested by a Vickers micro hardness tester (Duramin-2 of Struers). Moreover, a tensile tester (Instron 3T, Model 5967B12620) was employed to implement all tensile tests. The tests of tensile strengths had been conducted at ambient temperature. The traveling speed of the crosshead was set by 10 mm/min. In order to evaluate the defects of components, all metallurgical samples (MS-*i*) and tensile samples were tested through the X-ray CT tests.

3 Findings and Discussion

The X-ray CT photographs of MS and tensile samples are shown in Fig. 2, in which defects generally appear in black color, whereas the parts appear in bright color. It is found that there are no black zones observed in the microstructure testing samples and the tensile samples. Therefore, we can consider that the walls were successfully produced by WAAM without major defects such as macro porosity and cracks.

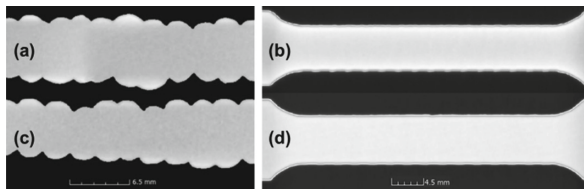


Fig. 2. X-Ray CT photographs of the MS specimen and tensile samples of the first wall (a–b) and those of the second wall (c–d).

Figure 3 presents the typical microstructure in the middle of the walls. It is firstly observed that the evolution of microstructure in two walls is almost identical. The microstructure of WAAM SS308L thin-walled components is composed of austenitic phases γ and ferrite δ remaining in the austenite grains' boundary.

In the middle of the walls, we can easily distinguish the microstructure evolution of each layer. Within a layer, austenite grains develop nearly vertically along the building direction. Cellular structures appeared close to the fusion line. They subsequently developed into finer columnar structures in the middle of the layer (Fig. 3a–c). The columnar structures gradually grew along the height of the layer. They finally transformed into coarser granular grains in the layer's upper part (Fig. 3b). The secondary-dendrite arms are also clearly observed (Fig. 3a).

To analyze the impact of interpass-cooling times on the microstructure of the as-built walls, we measured the secondary dendrite arms' spacing (SDAS) at the same

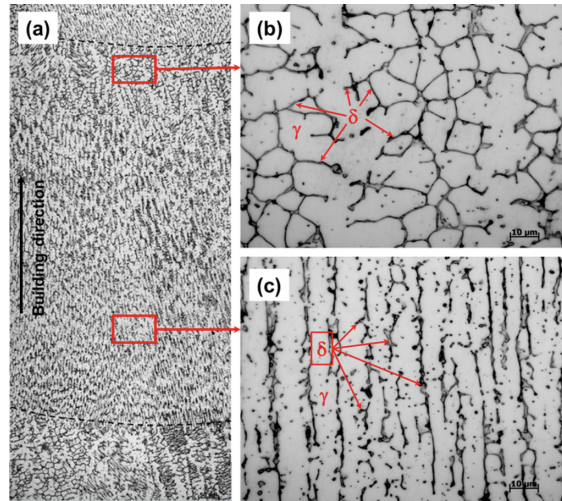


Fig. 3. Overall microstructures in the middle region (a) at low magnification (x100) of the as-built walls, and microstructure in the upper portion (b) and in other portions of a layer (c) in the middle region of the walls at high magnification (x500).

layer by using ImageJ software. In both two cases, it is found that the average SDAS augments in the height direction of the layer. In the case of the first wall ($T_{id} = 30$ s), the average SDAS is 8.20 ± 0.49 , 10.52 ± 0.33 , and $12.64 \pm 0.86 \mu\text{m}$ in the bottom, the middle, and the top of the layer, respectively. Moreover, the increase in the interpass-cooling time from $T_{id} = 30$ s to $T_{id} = 60$ s results in a decrease in SDAS. For instance, in the middle of the layer, the average SDAS is $10.52 \pm 0.33 \mu\text{m}$ and $9.62 \pm 0.54 \mu\text{m}$ for the first and the second wall, respectively. Indeed, due to the interlayer idle time increases, the interlayer temperature becomes lower, and the cooling rate increases [5, 7, 8]. As a result, the SDAS increases [7, 9].

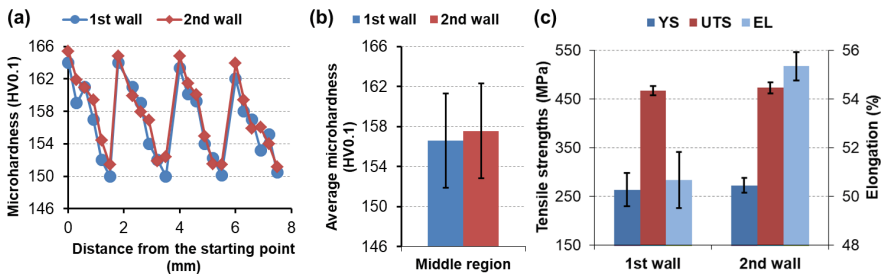


Fig. 4. Microhardness in the middle portion (a, b), and the tensile property (c) of the WAAM as-built material.

Figure 4a shows the microhardness distribution in four adjacent layers of the walls in the middle, and a comparison on the average hardness values between the walls was

described in Fig. 4b. It is found that the second wall features an average hardness that is higher than that of the first wall (157.62 ± 4.78 HV0.1 vs. 156.58 ± 4.71 HV0.1). Similarly, the second wall features the tensile strength that is superior to that of the first wall (Fig. 4c). The YS (yield strength), UTS (ultimate tensile strength), and EL (elongation) of the second wall are 275.67 ± 15.53 MPa, 472.33 ± 11.06 MPa, and $54 \pm 1\%$, respectively, whereas YS = 263.67 ± 33.65 MPa, UTS = 467.67 ± 9.29 MPa, and EL = $50.67 \pm 1.15\%$ for the first wall. The reason is that the SDAS of the first wall was greater than that of the second one. Therefore, in agreement with the Hall-Petch relationship [10], the hardness and tensile strength of the second wall are higher.

4 Conclusion

In this article, the impact of the interpass-cooling time on material properties of stainless steel 308L manufacture by WAAM was addressed. The obtained findings indicated that no remarkable difference in terms of the microstructure evolution was observed between the walls built with different interlayer idle times. The microstructure of WAAM thin-walled SS308L components is mainly composed of austenite phases and residual ferrite in the austenite boundaries. The microhardness and tensile strength of as-built thin-walled components can be improved by increasing the interpass-cooling time between successive deposited layers. However, it is noted that the increase in the interpass-cooling time causes a loss in productivity.

Acknowledgements. This research is funded by Vietnam National Foundation for Science and Technology Development (NAFOSTED) under grant number 107.99-2019.18.

References

1. Wu, B., Pan, Z., Ding, D., et al.: A review of the wire arc additive manufacturing of metals: properties, defects and quality improvement. *J. Manuf. Process.* **35**, 127–139 (2018)
2. Cunningham, C.R., Flynn, J.M., Shokrani, A., et al.: Invited review article: strategies and processes for high quality wire arc additive manufacturing. *Addit. Manuf.* **22**, 672–686 (2018)
3. Zhao, H., Zhang, G., Yin, Z., Wu, L.: Effects of Interpass-cooling time on thermal stresses in multipass multilayer weld-based rapid prototyping. *J. Manuf. Sci. Eng.* **135**, 011016 (2013)
4. Montevecchi, F., Venturini, G., Grossi, N., Scippa, A., Campatelli, G.: Idle time selection for wire-arc additive manufacturing: a finite element-based technique. *Addit. Manuf.* **21**, 479–486 (2018)
5. Lei, Y., Xiong, J., Li, R.: Effect of inter layer idle time on thermal behavior for multi-layer single-pass thin-walled parts in GMAW-based additive manufacturing. *Int. J. Adv. Manuf. Technol.* **96**, 1355–1365 (2018)
6. Le, V.T., Mai, D.S., Doan, T.K., Hoang, Q.H.: Prediction of welding bead geometry for wire arc additive manufacturing of SS308L walls using response surface methodology. *Transp. Commun. Sci. J.* **71**, 431–443 (2020)

7. Wang, L., Xue, J., Wang, Q.: Correlation between arc mode, microstructure, and mechanical properties during wire arc additive manufacturing of 316L stainless steel. *Mater. Sci. Eng. A* **751**, 183–190 (2019)
8. Yang, D., Wang, G., Zhang, G.: Thermal analysis for single-pass multi-layer GMAW based additive manufacturing using infrared thermography. *J. Mater. Process. Technol.* **244**, 215–224 (2017)
9. Yin, H., Felicelli, S.D.: Dendrite growth simulation during solidification in the LENS process. *Acta Mater.* **58**, 1455–1465 (2010)
10. Singh, K.K., Sangal, S., Murty, G.S.: Hall-Petch behaviour of 316L austenitic stainless steel at room temperature. *Mater. Sci. Technol.* **18**, 165–172 (2002)